
B3: Stochastic modelling and deterministic limit of catalytic surface processes

J. Starke¹, C. Reichert², M. Eiswirth³, and K. Oelschläger⁴

¹ Institute of Applied Mathematics & Interdisciplinary Center for Scientific Computing, University of Heidelberg,
`starke@iwr.uni-heidelberg.de`

² Interdisciplinary Center for Scientific Computing, University of Heidelberg,
`christian.reichert@iwr.uni-heidelberg.de`

³ Fritz-Haber-Institute of the Max Planck Society, Berlin,
`eiswirth@fhi-berlin.mpg.de`

⁴ Institute of Applied Mathematics, University of Heidelberg,
`karl.oelschlaeger@urz.uni-heidelberg.de`

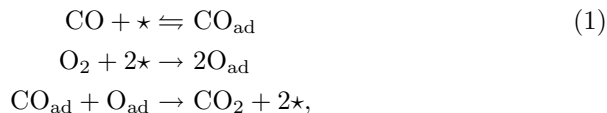
Three levels of modelling, microscopic, mesoscopic and macroscopic are discussed for the CO oxidation on low-index platinum single crystal surfaces. The introduced models on the microscopic and mesoscopic level are stochastic while the model on the macroscopic level is deterministic. It can be derived rigorously for low-pressure conditions from the microscopic model, which is characterized as a moderately interacting many-particle system, in the limit as the particle number tends to infinity. Also the mesoscopic model is given by a many-particle system. However, the state space there is a lattice, such that in contrast to the microscopic model the spatial resolution is reduced. The derivation of deterministic limit equations is in correspondence with the successful description of experiments under low-pressure conditions by deterministic reaction-diffusion equations while for intermediate pressures phenomena of stochastic origin can be observed in experiments. The models include a new approach for the platinum phase transition, which allows for a unification of existing models for Pt(100) and Pt(110). The rich nonlinear dynamical behaviour of the macroscopic reaction kinetics is investigated and shows good agreement with low pressure experiments. Furthermore, for intermediate pressures, noise-induced pattern formation, which has not been captured by earlier models, can be reproduced in stochastic simulations with the mesoscopic model.

1 Introduction

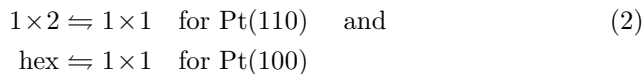
Stochastic modelling with many-particle systems and derivation of the corresponding deterministic limit is important in many areas of science. The present work concentrates on the CO oxidation on Pt single crystal surfaces but the techniques presented here can certainly be used in other areas as well.

1.1 CO oxidation on Pt single crystal surfaces

Pattern formation under nonequilibrium conditions has been studied using a number of catalytic surface reactions on a large variety of different catalysts [9, 10, 26]. In order to distinguish genuine self-organized patterns from influences of catalyst inhomogeneities, it is necessary to work with uniform surfaces; best suited are oriented single crystal surfaces. The system studied most extensively under these conditions is the CO oxidation on Pt single crystals [24, 8, 26, 37]. In ultra-high vacuum experiments, the elementary processes were elucidated. The reaction proceeds via the classical Langmuir-Hinshelwood mechanism,



where \star is a vacant adsorption site on the Pt surface. It is important to note that there is asymmetric inhibition of adsorption, i.e. preadsorbed CO blocks oxygen adsorption but not vice versa. In addition, the adsorbate-induced phase transition



has to be taken into account because the surface structure influences the reactivity.

The considered experimental situation assumes constant partial pressures of CO and O₂ in the well-mixed gaseous phase. The produced CO₂ disappears immediately from the Pt surface. It is therefore sufficient to model the adsorbed CO molecules and oxygen atoms on the Pt surface in addition to the platinum phase.

On a molecular level, the relevant elementary processes are of stochastic nature. Thus, fluctuations were shown to strongly influence the behavior in experiments with field emitter tips and corresponding Monte-Carlo simulations [42, 41]. In contrast, pattern formation on extended single crystal surfaces at low pressure ($\lesssim 10^{-4}$ mbar) did not reveal any effects which would suggest a stochastic origin, and could indeed be successfully modelled with (deterministic) reaction-diffusion equations [8].

The reason is that at low pressures there occur due to the diffusion of adsorbed CO on the Pt surface about 10^6 site changes per adsorption event, i.e. the surface is well mixed on a length scale of about $1\mu\text{m}$ and fluctuations on the molecular level are averaged out. With increasing pressure smaller and smaller patches can be regarded as well mixed, the size of a critical nucleus decreases [2]. The reaction-diffusion models are expected to fail and stochastic effects can become relevant. An experimental observation at an intermediate oxygen pressure ($p_{\text{O}_2} = 10^{-2}\text{mbar}$) is reproduced in Fig. 1. The CO pressure

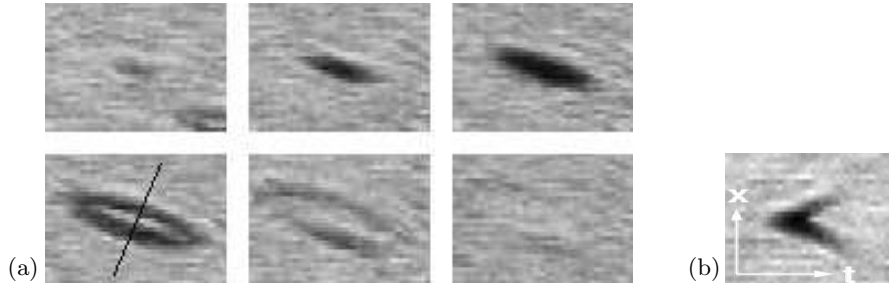


Fig. 1. (a) Snapshots of a Pt(110) single crystal surface showing the so-called raindrop patterns using EMSI (Ellipso Microscopy for Surface Imaging) [37]. The time between the snapshots is 160ms. The length scale is $100 \times 70\mu\text{m}$. The partial pressures are $p_{\text{CO}} = 7 \times 10^{-3}\text{mbar}$ and $p_{\text{O}_2} = 2.2 \times 10^{-2}\text{mbar}$. (b) Space-time diagram of the raindrop [37] showing $1.6\text{s} \times 100\mu\text{m}$.

p_{CO} had been stepwise increased to a point shortly before the whole surface would switch to the CO-covered state. CO nuclei were observed to originate at various places, forming a ring-shaped pattern, but were subsequently destroyed (propagation failure). These phenomena are called raindrop patterns due to the similarity to damped out waves on a water surface in starting rain. They seem to appear randomly distributed all over the catalyst surface [38].

Consequently, a unified stochastic model was developed which reproduces the meanfield limit at low pressures, but also describes the stochastic effects observed in experiments at intermediate pressure. In addition for these pressures, the reaction is no longer isothermal because the elevated turnover releases more heat, which is also included in the presented modelling.

1.2 Stochastic modelling and deterministic limit

Various types of many-particle models on small scales have been proposed to describe and analyse phenomena in science including fluctuations and other stochastic effects. To analyse the behaviour of those microscopically defined systems on macroscopic scales, it is useful to study the many-particle models in the limit as the particle number tends to infinity. A class of models

with strong local interaction essentially between immediately neighbouring particles leads to the so-called hydrodynamic limit [39, 5, 28]. On the other hand, models where any particle has a substantial albeit weak influence on essentially all other particles, i.e. models with global interactions lead to the so-called McKean-Vlasov limit [33]. To describe the experimental conditions of the CO oxidation on Pt considered in the present paper the limit behaviour of many-particle models exhibiting a local interaction with moderate interaction range which is much larger than the typical distance between neighbouring particles but much smaller than the total system size has to be studied. This results in a situation inbetween the hydrodynamic and the McKean-Vlasov limit.

In the following we present and investigate two types of these stochastic models with local interactions between many mesoscopically neighboring particles, namely a stochastic lattice model, also known as box model or Gillespie model and a moderately interacting many-particle model in continuous space. Monte-Carlo or stochastic cellular automaton models are not considered, as they are usually not able to reproduce with today's computer simulations the experimentally observed phenomena with realistic parameters.

Examples of stochastic lattice models using cells as spatial discretization can be found in [18] and [15]. Some analysis of these models has been based on the Master equation while a mathematically rigorous derivation of the deterministic limit was performed for chemical models assuming either specific reaction kinetics with at most quadratic terms or for systems with only one species specific polynomial kinetics [29, 30].

A rigorous derivation of the deterministic limit for particular many-particle models with moderate interaction, which model the evolution of biological populations, can be found in [34]. Applications of this approach have been employed to model the spatio-temporal pattern formation of myxobacteria [40] and to derive the Smoluchowski equation in the context of an astrophysical application [16].

The present paper is organized as follows: A mesoscopic lattice model for isothermal CO oxidation and its deterministic limit for the spatially homogeneous case are presented in Section 2. In Section 3 a limit theorem for a microscopic model, namely a moderately interacting many-particle system, is presented, which gives a rigorous result of the macroscopic reaction-diffusion equations as deterministic limit equations. The stochastic and thermokinetic effects which come into play at intermediate pressures are modelled in Section 4.

2 Stochastic lattice model for isothermal CO oxidation

The presented stochastic lattice model describes CO oxidation on Pt on a mesoscopic level with stochastic birth-death processes for the number of ad-

sorbed CO molecules, oxygen atoms and adsorption sites in (1×1) surface structure.

2.1 Model formulation and birth-death processes

Instead of distinguishing every single adsorption site like in microscopic Monte-Carlo simulations or in lattice gas approaches, the Pt surface is divided into a two-dimensional array or lattice of cells of mesoscopic size each containing N adsorption sites. Each cell is assumed to be well-mixed. The spatial resolution can thus be varied by changing N which automatically rescales the characteristic length. The state of a cell (i, j) containing N adsorption sites at time $t \geq 0$ is described by

$$\mathbf{X}_N^{(i,j)}(t) = \begin{pmatrix} N_{\text{CO}}^{(i,j)}(t) \\ N_{\text{O}}^{(i,j)}(t) \\ N_{1 \times 1}^{(i,j)}(t) \end{pmatrix} \in S_N^{(i,j)} = \{0, \dots, N\}^3, \quad (3)$$

where $N_{\text{CO}}^{(i,j)}$, $N_{\text{O}}^{(i,j)}$, and $N_{1 \times 1}^{(i,j)}$ denote for each cell (i, j) the numbers of CO molecules, oxygen atoms, and adsorption sites in a non-reconstructed (1×1) surface structure. The specific labels (i, j) of each cells are only printed for the considered interactions between cells. In order to characterize a stochastic process corresponding to the reaction mechanisms, transition probabilities to other states $P[\mathbf{X}_N(t+h) = \mathbf{X}_N(t) + \delta \mathbf{X}_N \mid \mathbf{X}_N(t)]$ for small h have to be specified. We introduce the concentrations $u_N := \frac{N_{\text{CO}}}{N}$, $v_N := \frac{N_{\text{O}}}{N}$, and $w_N := \frac{N_{1 \times 1}}{N}$; in the limit $N \rightarrow \infty$ they are denoted by u , v , and w .

The terms appearing below in the transition probabilities concerning N_{CO} and N_{O} essentially correspond to those used for the (deterministic) reconstruction model for Pt(110) in [31]. The parameters and rate constants are defined in Table 1. For further discussions see [31, 11, 25].

Adsorption

- Birth of a CO molecule on the surface.

$$N_{\text{CO}} \rightarrow N_{\text{CO}} + 1.$$

$$\begin{aligned} P[\mathbf{X}_N(t+h) = \mathbf{X}_N(t) + (1, 0, 0) \mid \mathbf{X}_N(t)] = \\ N p_{\text{CO}} \kappa_{\text{CO}} s_{\text{CO}} \left(1 - u_N^\xi(t)\right) h + o(h) \end{aligned} \quad (4)$$

- Birth of two adsorbed oxygen atoms.

$$N_{\text{O}} \rightarrow N_{\text{O}} + 2.$$

$$\begin{aligned} P[\mathbf{X}_N(t+h) = \mathbf{X}_N(t) + (0, 2, 0) \mid \mathbf{X}_N(t)] = \\ N p_{\text{O}_2} \frac{1}{2} \kappa_{\text{O}} \left(s_{\text{O}}^{\text{rec}} (1 - w_N(t)) + s_{\text{O}}^{1 \times 1} w_N(t)\right) \\ \times ((1 - u_N(t))(1 - v_N(t)))^2 h + o(h) \end{aligned} \quad (5)$$

By assuming the adsorption rate of CO to be proportional to $1 - u^\xi$ independent of the oxygen coverage as in [31], one implicitly drops the conservation constraint imposed on N_O , N_{CO} , and the number of vacant sites by the pure Langmuir-Hinshelwood mechanism. On the other hand, it has been observed experimentally that the presence of oxygen on the surface does not noticeably influence the adsorption of CO [26, 12]. Consequently, we assume that CO molecules can also be adsorbed at O-covered sites, whereas the dissociative adsorption of an oxygen molecule can only take place at two neighboring free sites. The probability that a particular site is occupied neither by CO nor by O is then $(1 - u)(1 - v)$ instead of $1 - u - v$ like it is used in [31]. Since the first term is larger only by uv , the difference is negligible if u or v is small (i.e. at low pressure). At intermediate pressure the new term is in better agreement with experiments [36].

The exponent ξ is introduced formally to model a precursor effect in the adsorption of CO as in [31], but it was always set to 1 in the present computations. Note that the sticking coefficient of oxygen on the 1×1 phase is higher than on the reconstructed phase which can lead to oscillatory, doubly metastable, and excitable behaviour of the reaction kinetics.

Desorption

- Death of a CO molecule through desorption.
 $N_{CO} \rightarrow N_{CO} - 1$.

$$P[\mathbf{X}_N(t+h) = \mathbf{X}_N(t) + (-1, 0, 0) \mid \mathbf{X}_N(t)] = N (k_{\text{des}}^{\text{rec}}(1 - w_N(t)) + k_{\text{des}}^{1 \times 1} w_N(t)) u_N(t) h + o(h) \quad (6)$$

The desorption of CO molecules from the reconstructed and the 1×1 phase has been distinguished here because the difference in the binding energies cannot be neglected in the case of Pt(100).

Reaction

- Death of a CO molecule and an oxygen atom through reaction.
 $N_{CO} \rightarrow N_{CO} - 1, N_O \rightarrow N_O - 1$.

$$P[\mathbf{X}_N(t+h) = \mathbf{X}_N(t) + (-1, -1, 0) \mid \mathbf{X}_N(t)] = N k_{\text{re}} u_N(t) v_N(t) h + o(h) \quad (7)$$

For a well-mixed patch the reaction probability is proportional to the product of the concentrations (mass action kinetics).

Phase transition

- Death of an adsorption site in a 1×1 patch and birth of a site in a reconstructed patch.
 $N_{1 \times 1} \rightarrow N_{1 \times 1} - 1$.

$$P[\mathbf{X}_N(t+h) = \mathbf{X}_N(t) + (0, 0, -1) \mid \mathbf{X}_N(t)] = Nk_{\text{rec}}f_{\text{rec}}(u_N(t), w_N(t))w_N(t)h + o(h) \quad (8)$$

- Death of a site in a reconstructed patch and birth of a site in a 1×1 patch.
 $N_{1 \times 1} \rightarrow N_{1 \times 1} + 1$.

$$P[\mathbf{X}_N(t+h) = \mathbf{X}_N(t) + (0, 0, 1) \mid \mathbf{X}_N(t)] = Nk_{1 \times 1}f_{1 \times 1}(u_N(t), v_N(t))(1-w_N(t))h + o(h), \quad (9)$$

where

$$f_{\text{rec}}(u_N, w_N) = (1-\epsilon)(1-u_N)^\lambda + \epsilon(1-w_N)^\lambda, \quad (10)$$

and

$$f_{1 \times 1}(u_N, w_N) = (1-\epsilon)u_N^\lambda + \epsilon w_N^\lambda, \quad \lambda > 1, \quad \epsilon \in [0, 1]. \quad (11)$$

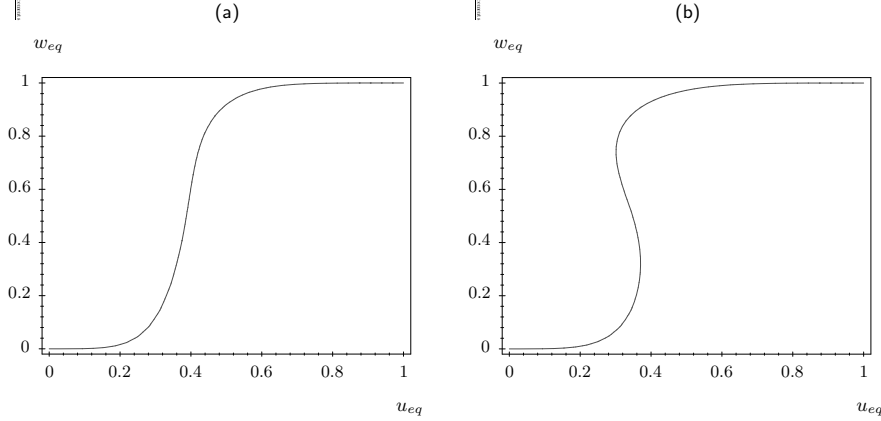


Fig. 2. Equilibria of the kinetics for $v \equiv 0$, $\frac{k_{\text{rec}}}{k_{1 \times 1}} = 0.2$, $\lambda = 4$, $k_{\text{des}}^{\text{rec}} = k_{\text{des}}^{1 \times 1}$, at different values of ϵ . (a) $\epsilon = 0.1$ (b) $\epsilon = 0.3$. Introducing different binding energies for CO on 1×1 - and reconstructed phase and thus a coupling between u and w , had almost no effect on the curves.

This ansatz is motivated by the fact that the phase transition proceeds via nucleation and growth. The probability for nucleation is determined solely by the CO coverage, but the growth of a phase can to some extent be autocatalytic which leads to a dependence of the rate of growth on the concentration

of the phase itself. Therefore we choose e.g. for the growth rate of the 1×1 phase on a reconstructed surface a weighted sum of u and w to some power λ , respectively (cf. eqs. (10) and (11)). A highly nonlinear dependence of this rate on u has been obtained experimentally by Hopkinson et al. [23]. They measured the growth rate of the 1×1 phase on a hex-R reconstructed Pt(100) surface to depend on the CO coverage on the hex-R phase to a power of about 4.5. It is plausible that the exponent for w should be of the same order of magnitude. The reverse transition is modelled in an analogous way. In order not to introduce too many parameters, the same ϵ and λ are used, however, the rate constants are allowed to be different.

The effect of the weight ϵ is shown in Fig. 2. For $\epsilon = 0.1$, the equilibrium portion of 1×1 phase can be expressed as a function of u_{eq} , as expected (cf. Fig. 2a). At higher values of ϵ both phases are stable within a certain range of u_{eq} (cf. Fig. 2b).

Diffusion

- Diffusive jump processes of a CO molecule in cell (i, j) to neighboring cells.

$$\begin{pmatrix} N_{\text{CO}}^{(i,j)} \\ N_{\text{CO}}^{(i+\Delta i, j+\Delta j)} \end{pmatrix} \rightarrow \begin{pmatrix} N_{\text{CO}}^{(i,j)} - 1 \\ N_{\text{CO}}^{(i+\Delta i, j+\Delta j)} + 1 \end{pmatrix} \text{ with } \begin{pmatrix} \Delta i \\ \Delta j \end{pmatrix} \in \left\{ \begin{pmatrix} \pm 1 \\ 0 \end{pmatrix}, \begin{pmatrix} 0 \\ \pm 1 \end{pmatrix} \right\}.$$

$$P \left[\begin{pmatrix} \mathbf{X}_N^{(i,j)} \\ \mathbf{X}_N^{(i+\Delta i, j+\Delta j)} \end{pmatrix} (t+h) = \begin{pmatrix} \mathbf{X}_N^{(i,j)} \\ \mathbf{X}_N^{(i+\Delta i, j+\Delta j)} \end{pmatrix} (t) + \begin{pmatrix} -1 \\ 0 \\ 0 \\ 1 \\ 0 \\ 0 \end{pmatrix} \right. \\ \left. \mid \begin{pmatrix} \mathbf{X}_N^{(i,j)} \\ \mathbf{X}_N^{(i+\Delta i, j+\Delta j)} \end{pmatrix} (t) \right] = N \frac{1}{4} D_{\text{CO}} u_N^{(i,j)}(t) + o(h) \quad (12)$$

Suitable boundary conditions have to be added. The diffusion of adsorbed oxygen is negligible.

Transition probabilities to other states behave like $o(h)$ (It is also assumed that the probability for a transition is zero if it would lead out of the state space.). Given an initial distribution for $\mathbf{X}_N^{(i,j)}(0)$, there is a Markov jump process in continuous time with state space S_N whose transition probabilities satisfy the above equations. Its paths can be chosen right-continuous with left limits. Because the state space S_N is bounded, explosions of particle numbers cannot occur, and the process is well-defined for $t \in [0, \infty)$ [3]. The time evolution of $P[\mathbf{X}_N^{(i,j)}(t) = \mathbf{Y}^{(i,j)} \mid \mathbf{X}_N^{(i,j)}(0) = \mathbf{X}_0^{(i,j)}]$, $\mathbf{Y}, \mathbf{X}_0 \in S_N$, is governed by a master equation [20, 19, 14, 22].

		Pt(110)	Pt(100)
CO adsorption			
impingement rate	κ_{CO}	$3.135 \times 10^5 \text{ mbar}^{-1} \text{ s}^{-1}$	$2.205 \times 10^5 \text{ mbar}^{-1} \text{ s}^{-1}$
sticking coefficient	s_{CO}	1	1
saturation coverage	u_s	1	1
precursor exponent	ξ	1	1
O ₂ adsorption			
impingement rate	κ_{O}	$5.858 \times 10^5 \text{ mbar}^{-1} \text{ s}^{-1}$	$3.75 \times 10^5 \text{ mbar}^{-1} \text{ s}^{-1}$
sticking coefficient	$s_{\text{O}}^{\text{rec}}$	0.3	0.001
	$s_{\text{O}}^{1 \times 1}$	0.6	0.3
saturation coverage	u_s	1	1
Arrhenius rates $\nu \exp(-\frac{E}{k_{\text{B}}T})$			
CO desorption	$k_{\text{des}}^{\text{rec}}$	$\nu_{\text{des}}^{\text{rec}} = 5 \times 10^{13} \text{ s}^{-1}$ $E_{\text{des}}^{\text{rec}} = 32.3 \text{ kcal/mol}$	$\nu_{\text{des}}^{\text{rec}} = 3.323 \times 10^{12} \text{ s}^{-1}$ $E_{\text{des}}^{\text{rec}} = 27.5 \text{ kcal/mol}$
CO desorption	$k_{\text{des}}^{1 \times 1}$	$\nu_{\text{des}}^{1 \times 1} = 5 \times 10^{13} \text{ s}^{-1}$ $E_{\text{des}}^{1 \times 1} = 32.3 \text{ kcal/mol}$	$\nu_{\text{des}}^{1 \times 1} = 8.640 \times 10^{14} \text{ s}^{-1}$ $E_{\text{des}}^{1 \times 1} = 35.0 \text{ kcal/mol}$
reaction	k_{re}	$\nu_{\text{re}} = 5 \times 10^5 \text{ s}^{-1}$ $E_{\text{re}} = 8.1 \text{ kcal/mol}$	$\nu_{\text{re}} = 1.185 \times 10^9 \text{ s}^{-1}$ $E_{\text{re}} = 14 \text{ kcal/mol}$
phase transition	$k_{1 \times 1}$	$\nu_{1 \times 1} = 10^3 \text{ s}^{-1}$ $E_{1 \times 1} = 6.9 \text{ kcal/mol}$	$\nu_{1 \times 1} = 2.417 \times 10^{11} \text{ s}^{-1}$ $E_{1 \times 1} = 25 \text{ kcal/mol}$
	k_{rec}	$\nu_{\text{rec}} = 0.2 \times 10^3 \text{ s}^{-1}$ $E_{\text{rec}} = 6.9 \text{ kcal/mol}$	$\nu_{\text{rec}} = 4.833 \times 10^{10} \text{ s}^{-1}$ $E_{\text{rec}} = 25 \text{ kcal/mol}$
phase transition			
exponent	λ	4	4
weight	ϵ	0.1	0.3

Table 1. Kinetic parameters for Pt(110) and Pt(100).

2.2 Deterministic Limit

To investigate the dynamical properties of the model it is convenient to use the deterministic limit of the introduced many-particle model. The deterministic limit is given for the homogeneous case in the following.

We denote the stochastic processes describing the dynamics of the densities by

$$\mathbf{x}_N(t) = \frac{1}{N} \mathbf{X}_N(t) = \begin{pmatrix} u_N(t) \\ v_N(t) \\ w_N(t) \end{pmatrix}. \quad (13)$$

Note that all transition intensities (cf. eqs. (4-9)) are proportional to a product of the system size N and a function of the concentrations only. Because of this scaling property it can be proved rigorously that, if $\lim_{N \rightarrow \infty} \mathbf{x}_N(0) = \mathbf{x}_0 \in [0, 1]^3$ holds with probability one, the paths of the stochastic processes $\mathbf{x}_N(t)$ approximate the solution $\mathbf{x}(t)$ of the initial value problem given by the system of ODEs

$$\begin{aligned}
\dot{u} &= p_{\text{CO}}\kappa_{\text{CO}}s_{\text{CO}}(1-u^\xi) - (k_{\text{des}}^{\text{rec}}(1-w) + k_{\text{des}}^{1\times 1}w)u - k_{\text{re}}uv \\
\dot{v} &= p_{\text{O}_2}\kappa_{\text{O}}(s_{\text{O}}^{\text{rec}}(1-w) + s_{\text{O}}^{1\times 1}w)((1-u)(1-v))^2 - k_{\text{re}}uv \\
\dot{w} &= k_{1\times 1}f_{1\times 1}(u,w)(1-w) - k_{\text{rec}}f_{\text{rec}}(u,w)w,
\end{aligned} \tag{14}$$

and the initial condition $\mathbf{x}(0) = \mathbf{x}_0$ at large particle numbers in the following sense:

$$\text{For arbitrary } t \geq 0: \quad \lim_{N \rightarrow \infty} \sup_{0 \leq s \leq t} |\mathbf{x}_N(s) - \mathbf{x}(s)| = 0 \quad \text{with probability one.}$$

In addition, a central limit theorem can be shown which states that fluctuations of the concentrations vanish like $O(\frac{1}{\sqrt{N}})$. The proofs follow directly from theorems by Kurtz [32, 13]. A non-rigorous approach to these results is known in the physical literature as van Kampen's system size expansion [14].

Bifurcation analysis

Subsequently we present some aspects of the bifurcation structure of system (14) with parameters appropriate for Pt(110) and Pt(100). For a more complete treatment see [36]. The computations were performed using algorithms contained in the AUTO 97 package by Doedel et al. [6]. Abbreviations of the bifurcations found are listed in Table 2, for details see [21, 43, 17].

For Pt(110), bifurcation diagrams in p_{CO} and p_{O_2} have been computed for several fixed sample temperatures. The kinetic parameters used are listed in Table 1.

At higher temperatures (500 K–560 K) the bifurcation diagram is mainly organized by a cusp and two Takens-Bogdanov points. In total there are 12 parameter regions with different dynamical behaviour (cf. Fig. 3), but only regions 1–5 are physically relevant because the remaining regions are too small to be detected in typical experiments. In areas 1, 2, and 3 there is only one attractor, a stable node and an asymptotically stable periodic orbit, respectively. The maximal width of the oscillatory region 2 at 540 K amounts to $\approx 10\%$ of the value of p_{CO} at the supercritical Hopf bifurcation. It decreases towards higher as well as lower temperatures. In 4 and 5 two attractors coexist; in 5 there are two stable nodes, while in 4 the system reaches either a stable node or a small asymptotically stable periodic orbit. The width of region 4 is $\lesssim 1\%$ of p_{CO} at 540 K, so it could possibly be detected experimentally. The areas with nontrivial dynamics, such as bistability or oscillations, move towards higher partial pressures as temperature is increased.

Phase portraits of the dynamics in the different parameter regions are sketched in Fig. 3. In the pictures containing three fixed points the lower one can always be identified with a reactive, only partially non-reconstructed surface with a relatively high oxygen coverage (reactive state), the upper one with a mainly CO-covered 1×1 surface (poisoned state).

From a physical point of view the model presented here yields almost the same results as the one proposed in ref. [31]. The most important distinction

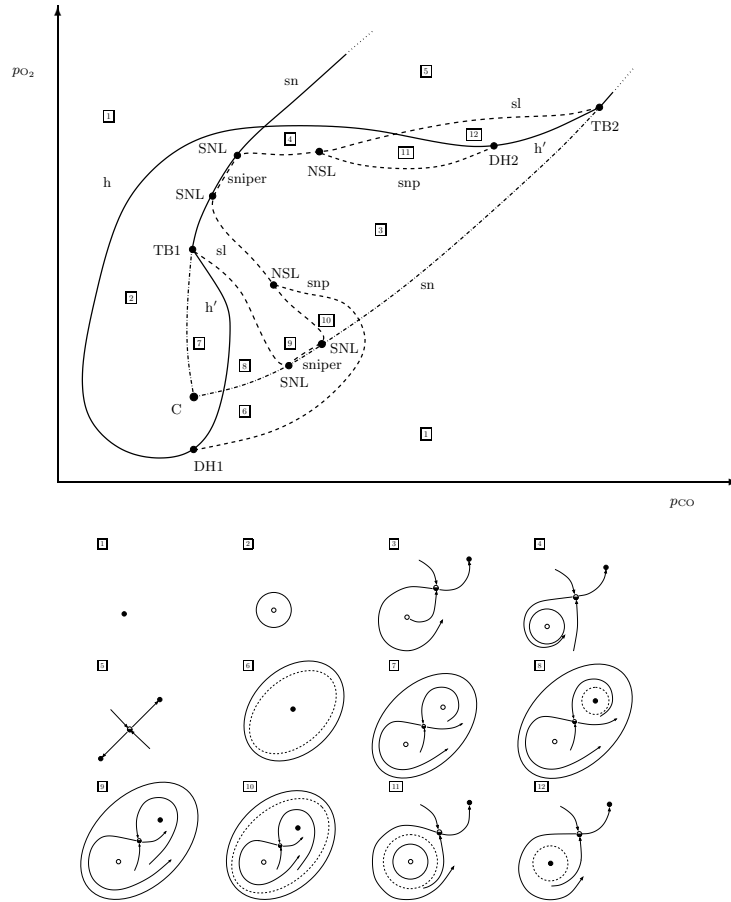


Fig. 3. Sketches of the complete bifurcation diagram at 500 K–560 K (top) and phase portraits in different parameter regions (bottom) for Pt(110). Hopf bifurcations, and saddle-node bifurcations involving a stable node and a saddle with a one-dimensional unstable manifold are drawn with solid lines, saddle-node bifurcations involving a saddle with a one-dimensional and another with a two-dimensional unstable manifold are drawn with dash-dotted lines. The dashed curves indicate global bifurcations, cf. Table 2. In the phase portraits stable nodes are represented by filled circles, saddle points with a two-dimensional unstable manifold by empty circles, and saddle points with a one-dimensional unstable manifold by half-filled circles. Asymptotically stable periodic orbits are indicated by solid lines, unstable ones by dashed lines.

is that here the two curves of saddle-node bifurcations do not merge for the investigated parameter region in a second cusp when p_{CO} and p_{O_2} are increased, rather bistability persists even at atmospheric pressures, in agreement with

Bifurcation	Codimension	Abbreviation
Hopf bifurcation (supercritical)	1	h
Hopf bifurcation (subcritical)	1	h'
saddle-node	1	sn
saddle loop homoclinic bifurcation	1	sl
saddle-node/infinite period saddle-node on a loop	1	sniper
saddle node of periodic orbits	1	snp
cusp	2	C
Takens-Bogdanov bifurcation	2	TB
degenerate Hopf bifurcation	2	DH
saddle-node loop	2	SNL
neutral saddle loop trace 0 saddle loop	2	NSL
Takens-Bogdanov-cusp	3	TBC

Table 2. Commonly used denotations of bifurcations and their abbreviations. By a degenerate Hopf bifurcation we mean the one described in [17].

experiment. In fact, this is due to the change of the adsorption kinetics of oxygen, as was checked by repeating the computation of the saddle-node curves with the term that was used in former models [31]. As in [31], the dynamics seems to be essentially two-dimensional; for instance a period doubling transition to chaos which was observed experimentally, could not be found.

In the case of Pt(100), the difference in the binding energies of CO on 1×1 - and hex phase must be taken into account. Moreover, some kinetic parameters have to be changed, most importantly the sticking coefficient of oxygen on the hex phase is much smaller than on the 1×2 phase of Pt(110). The weight ϵ is increased to $\epsilon = 0.3$, in order to model hysteresis in the phase transition; the influence of adsorbed oxygen on the restructuring processes has been neglected. The kinetic parameters used have been adapted from an older model [25]; they are listed in Table 1. For details of the bifurcation structure see [36].

The oscillatory region is much broader than in the case of Pt(110). It compares favourably with experiments (cf. Figs. 4a and 4b). In contrast to earlier models [25, 1] no arbitrary parameters have to be introduced through so-called defect terms to get the required behaviour. In contrast to Pt(110), Pt(100) exhibits two distinct bistable regions. The one at low pressures is due to the hysteresis in the phase transition and extends to zero oxygen pressure, while the one at high pressures is controlled by the reaction dynamics and again does not close. Overall, the bifurcation fine structure turned out somewhat simpler than with Pt(110).

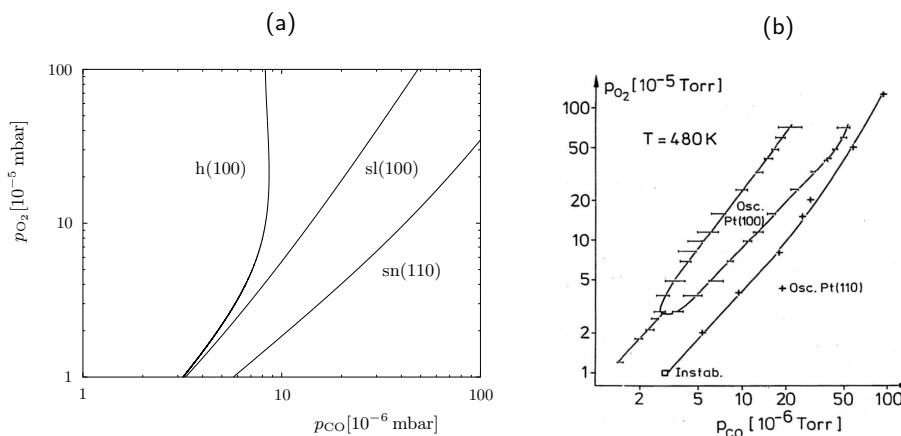


Fig. 4. Occurrence of oscillations at 480 K. (a) The curves of Hopf- and sl bifurcations are plotted for Pt(100) using a logarithmic scale. The line on the right is the curve of saddle-node bifurcations corresponding to the loss of stability of the reactive state for Pt(110). (b) Corresponding experimental diagram [11].

3 Limit theorem for many-particle systems in continuous space

In this Section, which summarizes [35], the relationship between two different approaches to the mathematical modelling of general chemical systems with intermediate particle interactions, i.e. with microscopically large and macroscopically small range, is investigated. In particular, the rigorous derivation of macroscopic limit equations (reaction-diffusion equations) from microscopic moderately interacting many-particle models is discussed.

3.1 Microscopic and macroscopic modelling of chemical reactions

For a large number of complex chemical systems, like the CO oxidation on Pt, the elementary reaction steps are understood, i.e., the microscopic dynamics of the chemical components is known. In contrast to this, many models describing macroscopic phenomena like spatio-temporal pattern formation should be improved, or, at least, their foundation on the microscopic description has to be supplemented.

In order to model particular chemical reactions on a microscopic level we consider a class of interacting many-particle systems. Especially, we focus on the use of moderately interacting many-particle systems, where for large particle numbers the mean distance between neighbouring particles is much smaller than the range of the interaction, which in turn is much smaller than the spatial system size. This is fulfilled for many important chemical reactions, where the dynamics is reaction- rather than diffusion-controlled. These systems can

be regarded as being locally well-mixed. To distinguish the model from the stochastic lattice model described in Section 2 we use the term “microscopic model” for the approach in this section because the positions of individual particles are considered here in continuous space and not on a discrete lattice which corresponds to a reduced spatial resolution. Nevertheless, by using densely populated cells or a moderately scaled interaction, both models are associated with a local averaging in connection with the respective interaction.

Similarly as in [34] we study for any $N \in \mathbb{N}$ a system of $\approx N$ particles in \mathbb{R}^d . To model different reacting species the set of all particles is divided into a finite collection of K subsets, where K is independent of N . The dynamics of the individual particles is determined by three contributions, namely

- immigration, i.e., the entering of new particles into the system e.g. by adsorption of a gaseous species on a surface,
- reaction, i.e., the transformation of pairs of interacting particles into particles of another species, and
- diffusion.

As far as the interaction among the particles is concerned, we suppose similarly as in [34] that immigration- and reaction rates depend on regularized versions of the empirical processes (16) of the various species. For fixed $N \in \mathbb{N}$ these regularizations are defined as convolutions of the respective empirical processes with a kernel ψ_N . Additionally, in our model the reaction rates involve some interaction potential ϕ_N describing the influence of the distance between the reacting particles, i.e., pair-interaction is included. With δ_0 denoting Dirac’s δ -distribution we assume that

$$\lim_{N \rightarrow \infty} \psi_N = \lim_{N \rightarrow \infty} \phi_N = \delta_0 \quad \text{in } \mathcal{S}'(\mathbb{R}^d) \text{ sufficiently slow.} \quad (15)$$

The rate of convergence in (15) has to be slow enough, in particular, in order that the various contributions to the interaction scale in a moderate way and hence moderately interacting many-particle systems are obtained, cf. [34]. In contrast to [34], in the model discussed here the diffusion may vanish for certain species. Moreover, no drift is acting on the particles. Last not least, the analysis in [34] is simplified considerably by the absence of explicit pair-interaction.

We are aiming at the study of the many-particle systems for large particle numbers, i.e., we investigate the limit $N \rightarrow \infty$. Especially, the convergence of the systems of empirical processes to the solution of a system of reaction-diffusion equations will be proved. This limit system represents a macroscopic model of the respective chemical reaction.

As an important application the particular example of the heterogeneous catalytic CO oxidation on Pt is considered for low pressures. The already mentioned 10^6 site changes of an adsorbed CO molecule per adsorption event due to diffusive hopping results in a locally well-mixed system. The asymmetric inhibition as well as the dynamical adsorbate dependent reconstruction of

the Pt structure can fully be considered also in this microscopic moderately interacting many-particle model. The description of this interesting surface reaction with its complicated spatio-temporal dynamical behaviour (cf. Section 2.2 for a numerical bifurcation analysis of the kinetics) is a suitable test for the proposed abstract chemical model. The mathematical modelling in this example including specific rates for the physical processes is presented in Section 3.5. Additionally, the corresponding system of partial differential equations for the macroscopic model is given there.

Sections 3.2 and 3.3 contain mathematical details for the general microscopic model and a limit theorem describing its relation to the corresponding macroscopic model. In Section 3.4 some remarks on the proof of the limit theorem can be found.

3.2 Mathematical details of the microscopic model for general reactions

For $N \in \mathbb{N}$ and $t \geq 0$ we use disjoint subsets $M_N^r(t)$, $r = 1, \dots, K$ of \mathbb{N} to describe the particles in the various subpopulations marked with r .

Let $X_N^k(t) \in \mathbb{R}^d$ be the position of particle k in the N -th system at time t . For fixed $N \in \mathbb{N}$ the distribution of the particles in space is characterized by empirical processes

$$\mathbb{X}_N^r(t) = \frac{1}{N} \sum_{k \in M_N^r(t)} \delta_{X_N^k(t)}, \quad t \geq 0, \quad r = 1, \dots, K, \quad (16)$$

which obviously take values in the space of nonnegative measures on \mathbb{R}^d .

The empirical processes will be used for two purposes:

- The reaction- and immigration rates describing the interaction between the particles depend on these processes.
- They are studied in the limit as $N \rightarrow \infty$ to determine the asymptotic behaviour of the many-particle systems.

To quantify the interaction the empirical processes \mathbb{X}_N^r are not employed directly. Instead, they are replaced by regularized versions ρ_N^r , which are obtained by convolving \mathbb{X}_N^r with some suitable kernel ψ_N , i.e.,

$$\rho_N^r(\cdot, t) = \mathbb{X}_N^r(t) * \psi_N, \quad t \geq 0, \quad r = 1, \dots, K, \quad N \in \mathbb{N}. \quad (17)$$

We suppose that the family ψ_N , $N \in \mathbb{N}$, is obtained by the scaling

$$\psi_N(x) = \theta_N \psi_1(\theta_N^{1/d} x), \quad x \in \mathbb{R}^d, \quad N \in \mathbb{N}, \quad (18)$$

where the function ψ_1 satisfying

$$\psi_1 \in C_b(\mathbb{R}^d; [0, \infty)), \quad \int_{\mathbb{R}^d} dx \psi_1(x) = 1, \quad \psi_1(-y) = \psi_1(y), \quad y \in \mathbb{R}^d, \quad (19)$$

is fixed. For the scaling coefficients θ_N , $N \in \mathbb{N}$, in (18) we suppose

$$\theta_1 = 1, \quad \theta_N \in [1, \infty), \quad N \in \mathbb{N}, \quad \lim_{N \rightarrow \infty} \theta_N = \infty \quad \text{sufficiently slow.} \quad (20)$$

It will be convenient to assemble ρ_N^r , $r = 1, \dots, K$, in the function $\rho_N : \mathbb{R}^d \times [0, \infty) \rightarrow [0, \infty)^K$ defined by

$$\rho_N(x, t) = (\rho_N^1(x, t), \dots, \rho_N^K(x, t)), \quad x \in \mathbb{R}^d, \quad t \geq 0. \quad (21)$$

As a further abbreviation we employ

$$\rho_N(x, y, t) = \frac{1}{2}(\rho_N(x, t) + \rho_N(y, t)), \quad x, y \in \mathbb{R}^d, \quad t \geq 0, \quad (22)$$

which will be utilized in the reaction rates.

Remark 1. Obviously, the transition from an empirical process \mathbb{X}_N^r to its regularization ρ_N^r may be considered as a spatial blurring of the point masses describing the positions of the individual particles. If this blurring is strong enough, i.e., if $\theta_N \rightarrow \infty$ sufficiently slow, cf. (20), it may be expected that asymptotically as $N \rightarrow \infty$ local fluctuations of mass concentrations vanish in ρ_N^r , and therefore $\rho = (\rho^1, \dots, \rho^K) = \lim_{N \rightarrow \infty} \rho_N$ should exist under rather general circumstances.

Now, for fixed $N \in \mathbb{N}$ the different contributions to the dynamics of the N -th many-particle system are described in detail.

To put our considerations involving random variables and stochastic processes on a firm basis we can work with a suitable filtered probability space $(\Omega, \mathcal{F}, (\mathcal{F}_t)_{t \geq 0}, \mathbf{P})$, where $(\mathcal{F}_t)_{t \geq 0}$ is some filtration satisfying the usual conditions, cf. [27]. We assume that any stochastic process appearing subsequently in this section is adapted to $(\mathcal{F}_t)_{t \geq 0}$.

Diffusion

We suppose that during their lifetimes the particles perform independent Brownian motions, where the diffusion constant is $\sigma_r \geq 0$, if the respective particle belongs to species r . Since the particles of certain species may be immobile, $\sigma_r = 0$ is allowed. To model the resulting paths of the particles independent standard \mathbb{R}^d -valued Brownian motions B_N^k , $k \in \mathbb{N}$, may be employed.

Immigration

It is assumed that particles may enter the system with density-dependent rates. More precisely, we suppose the existence of sufficiently regular functions

$$\beta^r \in C_b^1(\mathbb{R}^d \times [0, \infty)^K; [0, \infty)), \quad r = 1, \dots, K,$$

such that

$$\begin{aligned} \mathbf{P}[\text{a particle of species } r \text{ is immigrating in } U \text{ during } (t, t + \delta) | \mathcal{F}_t] & \quad (23) \\ & = \delta N \int_U dx \beta^r(x, \rho_N(x, t)) + o(\delta), \quad \text{as } \delta \searrow 0, \\ & \quad t \geq 0, \quad r = 1, \dots, K, \quad U \subseteq \mathbb{R}^d \text{ measurable.} \end{aligned}$$

Reaction

In nature various different types of reactions may occur. For notational simplicity we consider in our general model only the cases, where different particles of species r and r' can react to turn either into one particle of species p , or two particles of species p and p' , or three particles of species p , p' and p'' . Whereas r and r' are allowed to coincide, we assume that the species p , p' and p'' are different. As a consequence, for that type of reactions the species of the reaction products can be completely described by a set $B \in \Theta_3^K$, where Θ_3^K is the set of all subsets of $\{1, \dots, K\}$ with $1 \leq \text{card}(B) \leq 3$.

To model in the N -th system the influence of the spatial distance between two reacting particles on the reaction rate we use some kernel ϕ_N . As in (18) we assume that ϕ_N is obtained by a scaling

$$\phi_N(x) = \tau_N \phi_1(\tau_N^{1/d} x), \quad x \in \mathbb{R}^d, \quad N \in \mathbb{N}, \quad (24)$$

from some fixed function ϕ_1 . This function and the sequence $\tau_N, N \in \mathbb{N}$ are supposed to satisfy similar conditions as in (19) and (20).

To take into account catalytic effects we introduce functions

$$\beta_{r,r'}^B \in C_b^2([0, \infty)^K; [0, \infty)), \quad r, r' = 1, \dots, K, \quad B \in \Theta_3^K, \quad (25)$$

where the set B arising as upper index in $\beta_{r,r'}^B$ describes the species of the particles appearing after the reaction.

As in (23) we then assume

$$\begin{aligned} \mathbf{P} \left[\begin{array}{l} \text{particles } k \neq l \text{ of species } r \text{ and } r' \text{ located in } x \text{ and } y \text{ react} \\ \text{during } (t, t + \delta) \text{ to yield particles of species given by } B \end{array} \middle| \mathcal{F}_t \right] & \quad (26) \\ & = \frac{\delta}{N} \phi_N(x - y) \beta_{r,r'}^B(\rho_N(x, y, t)) + o(\delta), \quad \text{as } \delta \searrow 0, \\ & \quad x, y \in \mathbb{R}^d, \quad t \geq 0, \quad r, r' = 1, \dots, K, \quad B \in \Theta_3^K, \end{aligned}$$

where ρ_N is introduced in (17), (21) and (22). Moreover, we suppose that all particles resulting from a reaction between particles in $x, y \in \mathbb{R}^d$ emerge at the same point $(x + y)/2$.

Remark 2. In particular cases it can happen that certain reaction products do not contribute to further reactions, i.e., actually, they leave the system under consideration. This situation would correspond to $B = \emptyset$.

To drop the restriction to at most three particles resulting from any reaction or the assumption that the species of these particles are different we should assume that B is an arbitrary subset or an unordered tuple of elements of $\{1, \dots, K\}$.

Also splitting reactions, where one particle is divided into several fragments belonging to different species, are possible. For such reactions we may introduce additional reaction rates β_r^B , $r = 1, \dots, K$, B a subset or an unordered tuple of elements of $\{1, \dots, K\}$, in (25).

Apart from some trivial modifications our mathematical considerations in [35] also remain valid for the generalizations mentioned in this remark.

3.3 A limit theorem

The relationship between the microscopic model, i.e., the many-particle system described in Section 3.2, and its macroscopic equivalent, i.e., a nonlinear system of partial differential equations, is specified by the subsequent result.

Theorem 1. *Suppose that suitable regularity conditions are satisfied. Then,*

$$\lim_{N \rightarrow \infty} \sup_{t \leq T^*} |\langle \mathbb{X}_N^r(t), f \rangle - \langle \rho^r(\cdot, t), f \rangle| = 0, \quad \text{in probability,} \quad (27)$$

$$r = 1, \dots, K, \quad f \in C_b^1(\mathbb{R}^d) \cap L^2(\mathbb{R}^d),$$

where the limit densities collected in the $[0, \infty)^K$ -valued function $\rho = (\rho^1, \dots, \rho^K)$ solve

$$\begin{aligned} \frac{\partial}{\partial t} \rho^r(x, t) &= \beta^r(x, \rho(x, t)) - \sum_{r'=1}^K \sum_{B \in \Theta_3^K} \rho^r(x, t) \rho^{r'}(x, t) \beta_{r, r'}^B(\rho(x, t)) \quad (28) \\ &+ \frac{1}{2} \sum_{r', r''=1}^K \sum_{\{B \in \Theta_3^K : r \in B\}} \rho^{r'}(x, t) \rho^{r''}(x, t) \beta_{r', r''}^B(\rho(x, t)) + \frac{\sigma_r^2}{2} \Delta \rho^r(x, t), \\ &x \in \mathbb{R}^d, \quad t \in [0, T^*], \quad r = 1, \dots, K. \end{aligned}$$

The regularity conditions needed for this theorem are stated in detail in [35]. First, we need various conditions on the scaling coefficients θ_N , τ_N , $N \in \mathbb{N}$, which appear in (18) and (24), and further coefficients a_N , p_N , $N \in \mathbb{N}$. Next, the interaction kernels, ψ_1 , ϕ_1 , cf. (18) and (24), and the kernel W_1 , cf. (30) and (31) in Section 3.4, have to be regular enough. Finally, the solution (ρ^1, \dots, ρ^K) of the limit equation (28) should be sufficiently smooth in the time interval $[0, T^*]$.

We note that a_N , p_N , $N \in \mathbb{N}$, and W_1 are needed for technical reasons, i.e., they have no meaning in the modelling but are employed to deduce the theorem mathematically rigorously.

3.4 Some remarks on the proof of the limit theorem

The proof is based on systems of stochastic differential equations

$$\begin{aligned}
 \langle \mathbb{X}_N^r(t), f(\cdot, t) \rangle &= \frac{1}{N} \sum_{k \in M_N^r(t)} f(X_N^k(t), t) \\
 &= \frac{1}{N} \sum_{k \in M_N^r(0)} f(X_N^k(0), 0) \\
 &\quad + \frac{1}{N} \int_0^t \int_{\mathbb{R}^d} \mathbb{J}_N^r(dx, ds) f(x, s) \\
 &\quad - \frac{1}{N} \int_0^t \sum_{r'=1}^K \sum_{B \in \Theta_3^K} \sum_{\substack{k \in M_N^r(s) \\ l \in M_N^{r'}(s)}} \rho_{N;r,r';k,l}^B(ds) f(X_N^k(s), s) \\
 &\quad + \frac{1}{2N} \int_0^t \sum_{r',r''=1}^K \sum_{\substack{B \in \Theta_3^K : r \in B \\ l \in M_N^{r'}(s) \\ l' \in M_N^{r''}(s)}} \rho_{N;r',r'';l,l'}^B(ds) f\left(\frac{X_N^l(s) + X_N^{l'}(s)}{2}, s\right) \\
 &\quad + \frac{\sigma_r^2}{2N} \int_0^t ds \sum_{k \in M_N^r(s)} \Delta f(X_N^k(s), s) \\
 &\quad + \frac{\sigma_r}{N} \int_0^t \sum_{k \in M_N^r(s)} \nabla f(X_N^k(s), s) \cdot B_N^k(ds) \\
 &\quad + \frac{1}{N} \int_0^t ds \sum_{k \in M_N^r(s)} \frac{\partial}{\partial u} f(X_N^k(s), u) \Big|_{u=s}, \\
 t \geq 0, r = 1, \dots, K, f \in C_b^{2,1}(\mathbb{R}^d \times [0, \infty)), N \in \mathbb{N},
 \end{aligned} \tag{29}$$

for the empirical processes to describe the dynamics of the many-particle systems.

In (29) we denote for $r = 1, \dots, K$ and $N \in \mathbb{N}$ by \mathbb{J}_N^r some random field in $\mathbb{R}^d \times [0, \infty)$, which describes the instants in space-time, where in the N -particle system particles of species r are immigrating. Moreover, for any $N \in \mathbb{N}$, $r, r' = 1, \dots, K$, $k \in M_N^r(\cdot)$, $l \in M_N^{r'}(\cdot)$ and $B \in \Theta_3^K$ the process $\rho_{N;r,r';k,l}^B$ marks that instant, where the particles k and l in the r -th and the r' -th species, respectively, interact to produce particles described by the set B .

As a first application of (29) some formal arguments can be used to guess the limit dynamics (28). In this context, we suppose that for any $t \geq 0$ the empirical processes $\mathbb{X}_N^1(t), \dots, \mathbb{X}_N^K(t)$ indeed converge to limits having smooth densities $\rho^1(\cdot, t), \dots, \rho^K(\cdot, t)$. Next, we represent the stochastic integrals on the right side of (29) as sums of a martingale and a process of bounded variation of first order. We then observe that the martingales vanish as $N \rightarrow \infty$ and

take into account (15). As a formal result, (29) turns into a weak version of (28).

Now, the empirical processes $\mathbb{X}_N^1, \dots, \mathbb{X}_N^K$ and their supposed respective limits ρ^1, \dots, ρ^K can be compared directly. For that purpose we introduce with

$$\mathbb{Q}_N(t) = \sum_{r=1}^K \|(\mathbb{X}_N^r(t) - \rho^r(\cdot, t)) * W_N\|_2^2, \quad t \geq 0, \quad N \in \mathbb{N}, \quad (30)$$

a family of stochastic processes, which describe for fixed N some L^2 -distance between the N -particle system and the limit ρ . In (30) we use kernels

$$W_N(x) = a_N W_1(a_N^{1/d} x), \quad x \in \mathbb{R}^d, \quad N \in \mathbb{N}, \quad (31)$$

where W_1 is a sufficiently regular probability density and $a_N \nearrow \infty$ as $N \rightarrow \infty$.

To investigate the asymptotics as $N \rightarrow \infty$ we employ (28) and (29) to deduce for any \mathbb{Q}_N , $N \in \mathbb{N}$, a stochastic differential equation describing its time evolution. After extensive, but fairly straightforward estimates of the various terms of this stochastic differential equation essentially Gronwall's Lemma can be used to verify that \mathbb{Q}_N vanishes as $N \rightarrow \infty$. In particular,

$$\lim_{N \rightarrow \infty} \mathbf{E} \left[1 \wedge r_N \sup_{t \leq T^*} \mathbb{Q}_N(t) \right] = 0 \quad (32)$$

for some suitable sequence r_N , $N \in \mathbb{N}$, with $\lim_{N \rightarrow \infty} r_N = \infty$ is obtained. Finally, (27) is a simple consequence of (32).

For the details of the proof of the theorem we refer to [35].

3.5 Application to heterogeneous catalysis: CO oxidation on Pt

As indicated in the introduction the general considerations on the modelling of chemical reactions with many-particle models in continuous space is applied here to the example of the CO oxidation on low-index Pt-surfaces in a low-pressure atmosphere, where the partial pressures of O_2 and CO are kept constant.

In the present context it is particularly important that for modelling purposes the use of moderately interacting many-particle systems is justified, as under the considered conditions a locally well-mixed system is given.

The description in Section 3.2 is translated into a moderately interacting many-particle system in continuous space \mathbb{R}^2 with three species, i.e., $d = 2$ and $K = 3$. For the N -particle system we may employ \mathbb{X}_N^1 , \mathbb{X}_N^2 and \mathbb{X}_N^3 for the empirical processes associated to the CO-molecules, O-atoms and Pt- 1×1 adsorption sites, respectively. As far as the Langmuir-Hinshelwood mechanism and the adsorbate induced Pt phase transition given in (1) and (2) are concerned, some particular subsets of physical processes are modelled in terms of immigration, namely the adsorption of CO and O_2 and the transition from Pt-rec to Pt- 1×1 . The corresponding immigration rates are β^1 , $\beta^{2,2}$ and β^3 . Since

the empirical processes related to oxygen describe O-atoms, the adsorption of O₂-molecules is related to another trivial extension of our model introduced in Section 3.2, namely the simultaneous immigration of two particles at the same place. For this reason the notation $\beta^{2,2}$ instead of β^2 is employed. The remaining reactions in (1) and (2), i.e., the desorption of CO, the creation of CO₂ and the transition from Pt-1×1 to Pt-rec, are described as reactions according to Section 3.2. For those cases, after taking into account in particular Remark 2, the reaction rates β_1^0 , $\beta_{1,2}^0$ and β_3^0 have to be specified.

To quantify the above-mentioned rates we use the considerations in Section 2 which is based on [36]. In particular, after some slight modifications we choose

$$\beta^1(x, \rho^1, \rho^2, \rho^3) = p_{\text{CO}} \kappa_{\text{CO}} s_{\text{CO}} H_1(1 - (\rho^1)^\xi) S(x), \quad (33a)$$

$$\beta^{2,2}(x, \rho^1, \rho^2, \rho^3) = p_{\text{O}_2} \kappa_{\text{O}} (s_{\text{O}}^{1 \times 1} \rho^3 + s_{\text{O}}^{\text{rec}} H_1(1 - \rho^3)) (H_1(1 - \rho^1) H_1(1 - \rho^2))^2 S(x) / 2, \quad (33b)$$

$$\beta^3(x, \rho^1, \rho^2, \rho^3) = k_{1 \times 1} f_{1 \times 1}(\rho^1, \rho^3) H_1(1 - \rho^3) S(x), \quad (33c)$$

$$\beta_1^0(\rho^1, \rho^2, \rho^3) = k_{\text{des}}^{1 \times 1} \rho^3 + k_{\text{des}}^{\text{rec}} H_1(1 - \rho^3), \quad (33d)$$

$$\beta_{1,2}^0(\rho^1, \rho^2, \rho^3) = k_{\text{re}}, \quad (33e)$$

$$\beta_3^0(\rho^1, \rho^2, \rho^3) = k_{\text{rec}} f_{\text{rec}}(\rho^1, \rho^3), \quad x \in \mathbb{R}^2, \rho^1, \rho^2, \rho^3 \in [0, \infty). \quad (33f)$$

The kinetic parameters κ_{CO} , s_{CO} , ξ , κ_{O} , $s_{\text{O}}^{1 \times 1}$, $s_{\text{O}}^{\text{rec}}$, $k_{1 \times 1}$, $k_{\text{des}}^{1 \times 1}$, $k_{\text{des}}^{\text{rec}}$, k_{re} and k_{rec} , which are strictly positive, are given in Table 1. p_{CO} and p_{O_2} denote the partial pressure of CO and O₂, respectively, in the gaseous phase above the Pt-surface. The function $f_{1 \times 1}$ defined in (10) is used with the densities ρ^1, ρ^2, ρ^3 which results in

$$f_{1 \times 1}(\rho^1, \rho^3) = (1 - \epsilon)(\rho^1)^\lambda + \epsilon(\rho^3)^\lambda, \quad \rho^1, \rho^3 \in [0, \infty), \quad (34a)$$

whereas for f_{rec} we have

$$f_{\text{rec}}(\rho^1, \rho^3) = (1 - \epsilon)(H_1(1 - \rho^1))^\lambda + \epsilon(H_1(1 - \rho^3))^\lambda, \quad \rho^1, \rho^3 \in [0, \infty). \quad (34b)$$

In (34) the constants $\epsilon \in [0, 1]$ and $\lambda > 1$ have to be chosen suitably, as it is described in Section 2.

The function $S(x)$ with spatial variable x in (33a) - (33c) is used to model the size of the Pt-surface, which is finite. We suppose

$$S \in C_b^1(\mathbb{R}^d; [0, 1]) \text{ with } S(x) = \begin{cases} 1, & \text{if } |x| \leq R, \\ 0, & \text{if } |x| \geq R', \end{cases}$$

for suitable constants $R' > R > 0$. In order to avoid negative rates in (33) and (34) the function $[0, 1] \ni u \rightarrow 1 - u$ from Section 2 is replaced by $[0, \infty) \ni u \rightarrow H_1(1 - u)$, where $H_1(v) = \max\{v, 0\}$, $v \in \mathbb{R}$.

In [36], only the spatially homogeneous situation was considered. In particular, the diffusive hopping of adsorbed CO-molecules mentioned in Section 3.1 is neglected. Here, we model that phenomenon in terms of independent Brownian motions acting on the CO-molecules with diffusion constant $\sigma_1 = \sqrt{2D}$ for some $D > 0$. Both adsorbed O-atoms and Pt-1×1 adsorption sites are considered as immobile, i.e., $\sigma_2 = \sigma_3 = 0$ is supposed.

To complete our mathematical model of this particular chemical reaction we still have to choose suitable kernels ψ_1 and ϕ_1 and associated scaling coefficients θ_N , $N \in \mathbb{N}$, and τ_N , $N \in \mathbb{N}$. Since present knowledge of the chemistry does not seem to impose restrictions, it suffices to take into account the regularity conditions mentioned in the theorem in Section 3.3.

By the particular form of the rates in (33) and (34) we obtain as limit dynamics the system

$$\begin{aligned} \frac{\partial}{\partial t} \rho^1 &= p_{\text{CO}} \kappa_{\text{CO}} s_{\text{CO}} (1 - (\rho^1)^\xi) S \\ &\quad - (k_{\text{des}}^{1 \times 1} \rho^3 + k_{\text{des}}^{\text{rec}} (1 - \rho^3)) \rho^1 - k_{\text{re}} \rho^1 \rho^2 + D \Delta \rho^1, \end{aligned} \quad (35a)$$

$$\frac{\partial}{\partial t} \rho^2 = p_{\text{O}_2} \kappa_{\text{O}} (s_{\text{O}}^{1 \times 1} \rho^3 + s_{\text{O}}^{\text{rec}} (1 - \rho^3)) ((1 - \rho^1)(1 - \rho^2))^2 S - k_{\text{re}} \rho^1 \rho^2, \quad (35b)$$

$$\frac{\partial}{\partial t} \rho^3 = k_{1 \times 1} f_{1 \times 1}(\rho^1, \rho^3) (1 - \rho^3) S - k_{\text{rec}} f_{\text{rec}}(\rho^1, \rho^3) \rho^3. \quad (35c)$$

We note that the function H_1 does not appear in (35) as a consequence of a maximum principle, which implies

$$0 \leq \rho^1(x, t), \rho^2(x, t), \rho^3(x, t) \leq 1, \quad x \in \mathbb{R}^2, t \geq 0,$$

if this condition is imposed for the initial time $t = 0$.

The obtained reaction-diffusion equation (35) can now be used as microscopically justified macroscopic model for subsequent analysis and numerical simulation. While this model is in excellent agreement with experiments over a wide parameter range, it will fail when stochastic effects become important, as discussed in the next section.

4 Stochastic and thermokinetic effects in CO oxidation

For increasing pressure, there are fewer and fewer diffusion sites changes of adsorbed species per adsorption event. Therefore the characteristic length over which the system can be regarded as well mixed decreases until the corresponding number of sites becomes so small that fluctuations have to be taken into account and the mean-field limit is not applicable any more.

Additionally, at intermediate pressures, the system is no longer isothermal due to heat release by the reaction. The temperature T can be modelled using

the heat balance equation [4] for a volume V of the catalyst with heat capacity C :

$$CV\dot{T} = Q_{\text{ad}}^{\text{CO}} + Q_{\text{des}}^{\text{CO}} + Q_{\text{ad}}^{\text{O}} + Q_{\text{re}} + Q_{\text{rad}} + Q_{\text{cond}}. \quad (36)$$

$Q_{\text{ad}}^{\text{CO}}$, Q_{ad}^{O} , $Q_{\text{des}}^{\text{CO}}$, and Q_{re} are the rates of production of heat energy through the reaction processes, Q_{rad} and Q_{cond} are the balances for the gain and loss of heat through radiation, conduction and the feedback system regulating the temperature during the experiments by electrical heating.

Linearising the equation by Taylor expansion around the temperature T_0 in the absence of any reaction and rescaling the temperature to $\theta = \frac{T-T_0}{T_0}$ leads to the equation

$$\begin{aligned} \dot{\theta} = \gamma \left\{ & (H_{\text{ad}}^{\text{CO}} \kappa_{\text{CO}} p_{\text{CO}} s_{\text{CO}} (1 - u^\xi) - H_{\text{des}}^{\text{CO}} k_{\text{des}}(\theta) u \right. \\ & + \frac{1}{2} H_{\text{ad}}^{\text{O}_2} \kappa_{\text{O}} p_{\text{O}_2} (s_{\text{O}}^{\text{rec}} (1 - w) + s_{\text{O}}^{1 \times 1} w) ((1 - u)(1 - v))^2 \\ & \left. + H_{\text{re}} k_{\text{re}}(\theta) uv \right\} - \mu \theta + D_\theta \nabla^2 \theta. \end{aligned} \quad (37)$$

Here γ represents a scaled heat capacity, the parameter μ contains the effectiveness of the feedback control:

$$\gamma(T_0) = \frac{\rho_s}{C \rho_b l_T T_0} \quad (38)$$

$$\mu(T_0) = \frac{4\sigma e_s(T_0) T_0^3 + \lambda_h / l_T}{C \rho_b l_T}. \quad (39)$$

The parameters entering these equations are summarized in Table 3.

The full deterministic model is obtained by the combination of equation (37) for the rescaled temperature with the reaction-diffusion equations

$$\begin{aligned} \dot{u} = & \kappa_{\text{CO}} p_{\text{CO}} s_{\text{CO}} (1 - u^\xi) - k_{\text{des}}(\theta) u - k_{\text{re}}(\theta) uv \\ & + D_{\text{CO}}(\theta) \nabla^2 u \end{aligned} \quad (40)$$

$$\begin{aligned} \dot{v} = & \kappa_{\text{O}} p_{\text{O}_2} (s_{\text{O}}^{\text{rec}} (1 - w) + s_{\text{O}}^{1 \times 1} w) ((1 - u)(1 - v))^2 \\ & - k_{\text{re}}(\theta) uv \end{aligned} \quad (41)$$

$$\dot{w} = k_{1 \times 1}(\theta) f_{1 \times 1}(u, w) (1 - w) - k_{\text{rec}}(\theta) f_{\text{rec}}(u, w) w. \quad (42)$$

and suitable boundary conditions. This macroscopic model (40) – (42) resulted in Section 3.5 in the interior of the bounded Pt surface (i.e. for $S(x) = 1$) as limit (35) from the moderately interacting many-particle model using temperature dependent Arrhenius rates $k(\theta) = \nu \exp(-\frac{E}{k_B T_0}) \exp(\frac{E}{k_B T_0} \frac{\theta}{1+\theta}) = \nu \exp(-\frac{E}{k_B T})$.

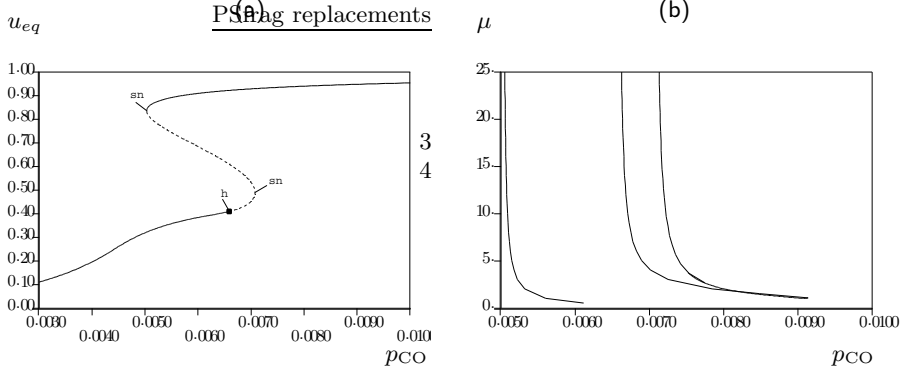
For large μ and not too high reaction rates the system would remain isothermal so that thermal effects can be analyzed using μ as bifurcation

$H_{\text{ad}}^{\text{CO}}$	heat of adsorption of CO	135 kJ mol ⁻¹
$H_{\text{des}}^{\text{CO}}$	heat loss by desorption of CO	$\approx H_{\text{ad}}^{\text{CO}}$
H_{re}	heat of reaction	20 - 30 kJ mol ⁻¹
$H_{\text{ad}}^{\text{O}_2}$	heat of adsorption of an oxygen atom	115 kJ mol ⁻¹
ρ_s	density of surface atoms	8.84×10^{18} atoms/m ²
σ	Stefan-Boltzmann constant	5.6705×10^{-8} Jm ⁻² K ⁻¹ s ⁻¹
e_s	integral emissivity of platinum	0.05 - 0.1
λ_h	heat conduction coefficient	72 W m ⁻¹ K ⁻¹
l_T	characteristic thickness of surface layer	5×10^{-5} m
C	specific heat capacity of platinum	130 J kg ⁻¹ K ⁻¹
ρ_b	bulk mass density of platinum	21.09×10^3 kgm ⁻³
D_θ	diffusion constant of temperature	$\lambda_h/(C\rho_b)$

Table 3. Parameters required for heat balance equation.

parameter. Thermokinetic effects are a consequence of the asymmetric inhibition of adsorption (i.e. preadsorbed CO blocks oxygen adsorption, but not vice versa) and the strong temperature dependence of CO desorption. Thus an O-covered surface exhibits a high reaction rate and therefore becomes hot while a high CO-coverage keeps the catalyst relatively cool. Since in turn lower T favors CO coverage through reduced desorption, the effect is autocatalytic.

A partial bifurcation analysis of the model is reproduced in Fig. 5. For

**Fig. 5.** (a) Continuation of CO coverage in p_{CO} for thermokinetic model. There is a Hopf bifurcation point (h) between two saddle-node bifurcation points (sn). (b) Continuation of Hopf and sn bifurcations in p_{CO} and μ .

large μ the O-covered surface is excitable close to the Hopf bifurcation and stable pulses exist. With decreasing μ this bifurcation shifts to higher p_{CO} , so

that the O-covered branch becomes subexcitable. Pulses can still be triggered, but they shrink and eventually vanish (Fig. 6). Physically this can be readily

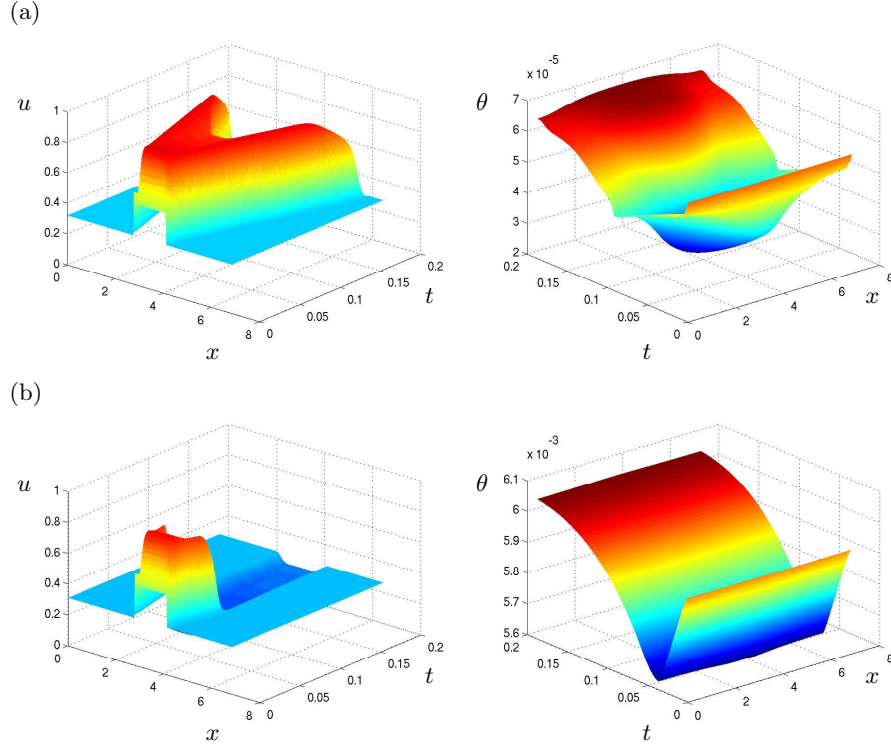


Fig. 6. Simulation of pulse propagation using thermokinetic model equations (40) – (42) and (37) in one dimension with rescaled temperature and no-flux boundary conditions. The space variable x is given in μm while the time t is given in s. A CO nucleus was put in the initial conditions on an otherwise predominantly O-covered surface. (a) For $\mu = 10^3$ pulses form, propagate but finally die due to rising temperature. (b) For $\mu = 10$ pulses can still be formed, but die quickly. $p_{\text{CO}} = 5.0 \times 10^{-3} \text{ mbar}$, $p_{\text{O}_2} = 1.55 \times 10^{-2} \text{ mbar}$, $D_{\text{CO}} = 10^{-12} \text{ m}^2/\text{s}$, $T_0 = 520 \text{ K}$, other parameters as in Tables 1 and 3. In the simulation shown heat conductance was chosen unrealistically small in order to visualize where heat production takes place. The effect of nucleation and propagation failure however persists even for a realistic heat diffusion (i.e. very large thermal conductivity).

explained by the temperature effects of the changes in reaction rate. The rate drops sharply on the (predominantly) CO covered areas, because here oxygen adsorption is blocked. However, behind the pulses the reconstruction has been lifted and the reactivity is increased to values even higher than on the original O-covered 1×2 surface because of the enhanced sticking coefficient

of oxygen on the 1×1 surface. Therefore, the temperature locally rises to values higher than at the beginning. Since the temperature spreads rapidly via heat conductance, the CO pulses are overrun from the inside (a hotter surface cannot maintain a high CO coverage due to enhanced desorption).

The stochastic model described in Section 2 was combined with thermokinetic effects using equation (37). Since heat conductance is much larger than diffusion, it was treated deterministically. For small pressures, the model behaved practically isothermally and followed the deterministic path very closely. In particular no spontaneous nucleation in the bistable or excitable region was observed. In contrast for parameters realistic for intermediate pressure ($N = 10^3$, hopping rate corresponding to $D_{\text{CO}} = 1.4 \times 10^{-14} \frac{\text{m}^2}{\text{s}}$) significant fluctuations become visible and critical nuclei did form spontaneously. A computer simulation for $p_{\text{O}_2} = 10^{-2} \text{mbar}$ of nucleation, pulse formation and propagation failure is reproduced in Fig. 7. The rate of such events turned out to be extremely sensitive with respect to p_{CO} . The nucleation was obviously random, the subsequent pulse annihilation occurred not too far from the deterministic path (cf. Fig. 6), although relatively small random variations in the maximum local CO coverage led to noticeable variations in the time it took to return to the initial state.

The homogeneous nucleation rate on an ideal surface can be roughly estimated using large-deviations analysis [7]. For an equilibrium CO coverage \bar{u} , a critical coverage u^* and a critical nucleus size containing n_{cr} sites, the system spends a time fraction of $\left[\left(\frac{\bar{u}}{u^*} \right)^{u^*} \left(\frac{1-\bar{u}}{1-u^*} \right)^{1-u^*} \right]^{n_{cr}}$ in a state with $u \geq u^*$.

u and u^* can be taken from the nullclines of the deterministic model, n_{cr} decreases linearly with the pressure and is between 10^3 and 10^4 at 10^{-2}mbar [2].

The expected number of events can be obtained by multiplying with the density of adsorption sites and dividing by the characteristic time, for which we chose the time required for the impingement of one monolayer CO. The resulting function is obviously very sensitive to n_{cr} but also depends crucially on $u^* - \bar{u}$. Reasonable values [37] of 1 to $100 \text{mm}^{-2} \text{s}^{-1}$ were obtained with $n_{cr} = 5000$, $u^* = 0.35$ and $0.31 < \bar{u} < 0.33$. Increasing n_{cr} by 2 orders of magnitude (which would correspond to a pressure decrease by 2 orders) resulted in values of about $10^{-35} \text{mm}^{-2} \text{s}^{-1}$ which would certainly not be observable in experiment nor computer simulations.

Obviously, surface inhomogeneities always play a role on real catalysts. Nevertheless, the experimental observations and their close correspondence to a realistic model clearly suggest that at least a significant fraction of the observed nuclei form uniformly distributed over the surface. The presented effect therefore constitutes the first example of mesoscopic pattern formation ($50 - 100 \mu\text{m}$) in a surface reaction that is initiated by microscopic fluctuations and cannot be fully captured in a deterministic description.

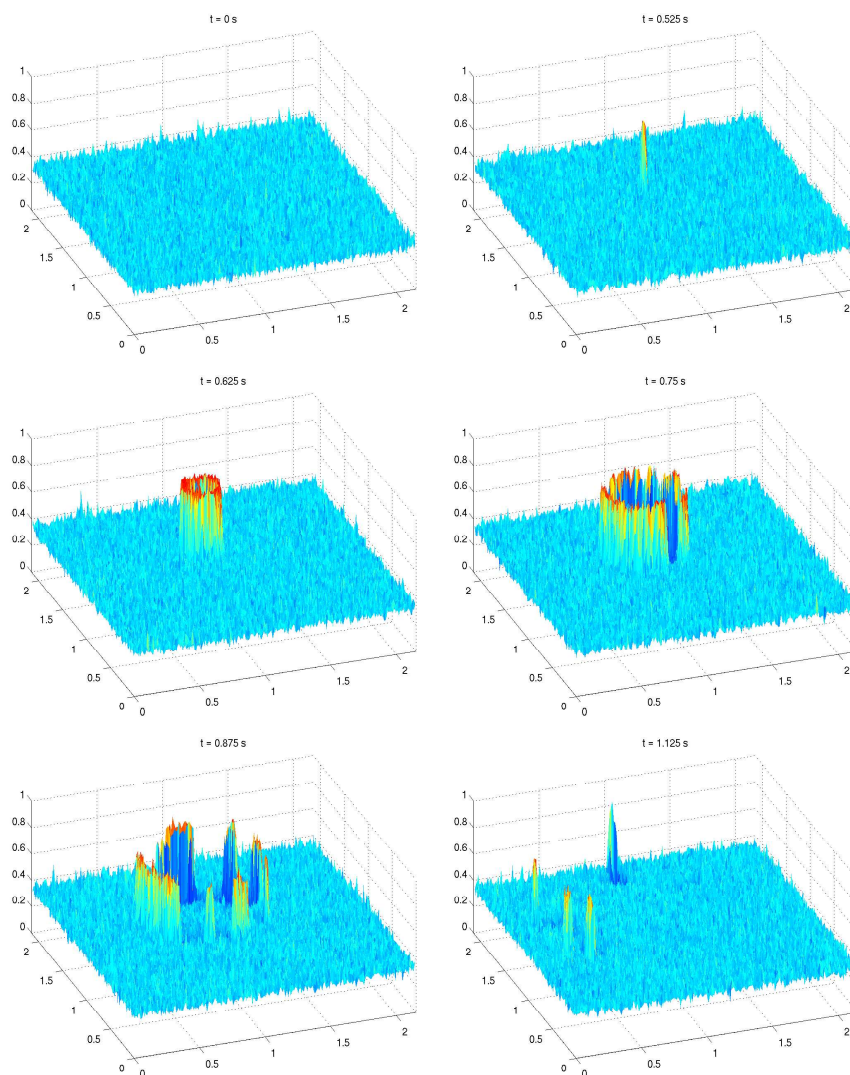


Fig. 7. Twodimensional simulation of raindrop patterns on a predominantly O-covered Pt(110) surface using stochastic model with included thermokinetic effects. CO nucleation occurred due to coverage fluctuations. For the stochastic simulation, 200×200 cells, $N = 10^3$ adsorption sites for each cell and $p_{\text{CO}} = 5.22 \times 10^{-3}$ mbar, $p_{\text{O}_2} = 1.55 \times 10^{-2}$ mbar, $D_{\text{CO}} = 1.4 \times 10^{-14} \text{m}^2/\text{s}$, $T_0 = 520 \text{K}$, $\mu = 10^3$ were used.

5 Conclusion

Spatio-temporal pattern formation in the CO oxidation on Pt has been studied experimentally over a wide range of parameters. The observed phenomena

mostly appear deterministically, except for very small catalyst areas or at sufficiently high pressure where also temperature variations become observable. In order to develop a consistent description of the large variety of experimental patterns, a unified stochastic model of CO oxidation including thermal effects for all low-index plane Pt surfaces was developed, which approaches a realistic deterministic limit when the surface can be regarded as well-mixed, but also reproduces stochastic effects with increasing pressure. It includes earlier models as limiting cases, i.e. approaches Monte-Carlo simulations for small cells and a reaction-diffusion system for intermediate particle interaction, and also reproduces stochastic effects, such as random nucleation.

References

1. R.F.S. Andrade, G. Dewel, and P. Borckmans. Modelling of the kinetic oscillations in the CO oxidation on Pt(100). *J. Chem. Phys.*, 91:2675–2682, 1989.
2. M. Bär, C. Zülicke, M. Eiswirth, and G. Ertl. Theoretical modeling of spatiotemporal self-organization in a surface catalyzed reaction exhibiting bistable kinetics. *Journal of Chemical Physics*, 96:8595 – 8604, 1992.
3. L. Breiman. *Probability*. Addison-Wesley, 1968.
4. J. Cisternas, P. Holmes, I. G. Kevrekidis, and X. Li. CO oxidation on thin Pt crystals: Temperature slaving and the derivation of lumped models. *Journal of Chemical Physics*, 118(7):3312 – 3328, 2003.
5. A. De Masi and E. Presutti. *Mathematical methods for hydrodynamic limits*. Lecture Notes in Mathematics, 1501. Springer-Verlag, 1991.
6. E. Doedel, A.R. Champneys, T.F. Fairgrieve, Y.A. Kusnetsov, B. Sandstede, and X. Wang. AUTO 97: Continuation and Bifurcation Software for Ordinary Differential Equations. <http://ftp.cs.concordia.ca/pub/doedel/auto>.
7. R. Durrett. *Probability: Theory and Examples*. Duxbury Press, Belmont, 1996.
8. M. Eiswirth, M. Bär, and H.H. Rotermund. Spatiotemporal selforganization on isothermal catalysts. *Physica D*, 84:40 – 57, 1995.
9. M. Eiswirth and G. Ertl. Kinetic oscillations in the catalytic oxidation of CO on Pt(110). *Surf. Sci.*, 90:177, 1986.
10. M. Eiswirth and G. Ertl. Pattern formation on Catalytic Surfaces. In R. Kapral and K. Showalter, editors, *Chemical Waves and Patterns*, page 447. Kluwer, Dordrecht, 1995.
11. Eiswirth, M. Phänomene der Selbstorganisation bei der Oxidation von CO an Pt(110). Dissertation, Ludwig-Maximilians-Universität München, 1987.
12. G. Ertl. Reaktionen an Festkörper-Oberflächen. *Berichte der Bunsengesellschaft*, 98:1413 – 1420, 1994.
13. Ethier, S.N., Kurtz, T.G. *Markov Processes: Characterization and Convergence*. Addison-Wesley, 1986.
14. C.W. Gardiner. *Handbook of Stochastic Methods*. Springer-Verlag, 1985.
15. D. Gillespie. Exact stochastic simulation of coupled chemical reactions. *The Journal of Physical Chemistry*, 81(25):2340 – 2361, 1977.
16. S. Großkinsky, C. Klingenberg, and K. Oelschläger. A rigorous derivation of smoluchowski's equation in the moderate limit. *Stochastic Anal. Appl.*, 22(1):113 – 141, 2004.

17. J. Guckenheimer. Multiple Bifurcation Problems for Chemical Reactors. *Physica D*, 20(1):1–20, 1986.
18. H. Haken. Statistical physics of bifurcation, spatial structures, and fluctuations of chemical reactions. *Zeitschrift für Physik B*, 20:413 – 420, 1975.
19. H. Haken. *Advanced Synergetics*. Springer Series in Synergetics. Springer-Verlag, Heidelberg, Berlin, New York, 1983.
20. H. Haken. *Synergetics, An Introduction*. Springer Series in Synergetics. Springer-Verlag, Heidelberg, Berlin, New York, 1983.
21. J. Hale and H. Koçak. *Dynamics and Bifurcations*. Springer-Verlag, Heidelberg, Berlin, New York, 1991.
22. J. Honerkamp. *Stochastic Dynamical Systems*. VCH, 1994.
23. A. Hopkinson, J.M. Bradley, X.-C. Guo, and D.A. King. Nonlinear Island Growth Dynamics in Adsorbate-Induced Restructuring of Quasihexagonal Reconstructed Pt(100) by CO. *Phys. Rev. Letters*, 71(10):1597–1600, 1993.
24. R. Imbihl. Temporal and spatial patterns in catalytic reactions on single crystal surfaces. *Heterogeneous Chemistry Reviews*, 1:125, 1994.
25. R. Imbihl, M.P. Cox, G. Ertl, H. Müller, and W. Brenig. Kinetic Oscillations in the Catalytic CO Oxidation on Pt(100): Theory. *J. Chem. Phys.*, 83(4):1578–1587, 1985.
26. R. Imbihl and G. Ertl. Oscillatory kinetics in heterogeneous catalysis. *Chemical Reviews*, 95(3):697 – 733, 1995.
27. I. Karatzas and S. E. Shreve. *Brownian Motion and Stochastic Calculus*. Springer-Verlag, Heidelberg, Berlin, New York, 1991.
28. Claude Kipnis and Claudio Landim. *Scaling limits of interacting particle systems*. Springer-Verlag, Heidelberg, Berlin, New York, 1999.
29. P. Kotelenez. Law of large numbers and central limit theorem for linear chemical reactions with diffusion. *The Annals of Probability*, 14(1):173 – 193, 1986.
30. P. Kotelenez. High density limit theorems for nonlinear chemical reactions with diffusion. *Probability Theory and Related Fields*, 78:11 – 37, 1988.
31. K. Krischer, M. Eiswirth, and G. Ertl. Oscillatory CO oxidation on Pt(110): Modeling of temporal self-organization. *Journal of Chemical Physics*, 96(12):9161 – 9172, 1992.
32. Kurtz, T.G. *Approximation of Population Processes*. Society for Industrial and Applied Mathematics, 1981.
33. S. Méléard. Asymptotic behaviour of some interacting particle systems – mckean-vaslov and boltzmann models. In D. Talay and L. Tubaro, editors, *Probabilistic Models for Nonlinear Partial Differential Equations*, Lecture Notes in Mathematics 1627, pages 42 – 95. Springer-Verlag, 1995.
34. K. Oelschläger. On the derivation of reaction-diffusion equations as limit dynamics of systems of moderately interacting stochastic processes. *Probability Theory and Related Fields*, 82:565 – 586, 1989.
35. K. Oelschläger and J. Starke. Many-particle models and reaction diffusion equations for chemical systems. Manuskript, 2004.
36. C. Reichert, J. Starke, and M. Eiswirth. Stochastic model of co-oxidation on platinum surfaces and deterministic limit. *Journal of Chemical Physics*, 115(10):4829 – 4838, 2001.
37. H. H. Rotermund. Imaging of dynamic processes on surfaces by light. *Surface Science Reports*, 29:265 – 364, 1997.
38. H. H. Rotermund. Imaging pattern formation in surface reactions from ultra-high vacuum up to atmospheric pressures. *Surface Science*, 386:10 – 23, 1997.

39. H. Spohn. *Large Scale Dynamics of Interacting Particles*. Springer-Verlag, 1991.
40. Angela Stevens. The derivation of chemotaxis equations as limit dynamics of moderately interacting stochastic many-particle systems. *SIAM J. Appl. Math.*, 61(1):183–212, 2000.
41. Yu. Suchorski, J. Beben, R. Imbihl, E.W. James, D.-J. Liu, and J.W. Evans. Fluctuations and Critical Phenomena in Catalytic CO-Oxidation on Pt Facets. *Physical Review B*, 63(16):165417, 2001.
42. Yu. Suchorski, J. Beben, E.W. James, J.W. Evans, and R. Imbihl. Fluctuation-induced transitions in a bistable surface reaction: Catalytic CO oxidation on a Pt field emitter tip. *Phys. Rev. Letters*, 82(9):1907–1910, 1999.
43. S. Wiggins. *Introduction to Applied Nonlinear Dynamical Systems and Chaos*. Springer-Verlag, Berlin, Heidelberg, New York, 1990.

